Available online at www.sciencedirect.com
ScienceDirect
Advances in Space Research 67 (2021) 1929–1936
ADVANCES IN SPACE RESEARCH (a COSPAR publication)
www.elsevier.com/locate/asr

Modeling the ionospheric gradient by using VSS base functions and GPS data over Iran

Hossein Etemadfard [a,*], Masoud Mashhadi Hossainali [b]

[a] Civil Engineering Department, Faculty of Engineering, Ferdowsi University of Mashhad (FUM), Mashhad, Iran
[b] Faculty of Geodesy and Geomatics Engineering, K. N. Toosi University of Technology, No. 1346, Vali_Asr Ave., Mirdamad Cr., Tehran, Iran

Received 30 April 2020; received in revised form 20 November 2020; accepted 18 December 2020
Available online 29 December 2020

Abstract

The spatial and temporal variations of ionosphere play an important role in positioning and navigation by the space geodetic techniques. Therefore, the ionospheric gradient should be calculated, analyzed, and applied in both space and time. Spatial gradients of the ionosphere have remarkable delay on the propagation of electromagnetic waves. This study intends to propose a new method for simultaneous modeling of the spatial gradients of ionosphere and VTECs in the local scale for Iran. Vector Spherical Slepian (VSS) base functions are used for the development of this method.

Five VSS models with the maximal degrees of $L = 30, 35, 40, 45$ and 50 are taken into account. For implementing the VSS method, 24 permanent GPS stations from the Iranian Permanent GPS Network (IPGN) have been used. The unknown coefficients are estimated with the observations of these stations with least squares technique. Four other stations are used for evaluating the accuracy of the models. Repeatability of baselines is the measure that is used for this purpose. Based on the results obtained, $L = 40$ is the optimum degree for the VSS model with this input data over Iran.

The baselines' repeatability showed that ionospheric gradients have more influence on the north–south component. Moreover, the spatial gradient is negligible in the east–west and up-down component when a short baseline is processed. In other words, this kind of ionospheric modeling has significant application for baseline, which is longer than 1000 km. In the study, proposed method has improved the long baselines' solution by more than 12%, 18% and 10% in east–west, north–south and up-down components, respectively.

Keywords: Slepian; Ionospheric Gradient; GPS observation

1. Introduction

The spatial and temporal variations of ionosphere play an important role in positioning and navigation by the space geodetic techniques (Danilogorskaya et al., 2017). In order to account for such variations, the ionospheric gradient should be calculated, analyzed, and applied in both space and time. The impact of ionospheric gradient has been studied on some of geodetic measurements (Meyer et al., 2005; Liu et al., 2003; Erickson et al., 2001) (see Fig. 1).

The gradient error effects on the relative positioning was first assessed by the Global Navigation Satellite System (GNSS) observations. Goad shows that the ionospheric gradient has about 0.5 m error on a long baseline in Antarctica (9 Km) during the maximum solar activity (Goad, 1990). Also, the ionospheric gradient of 5 m has been recorded on a baseline of 100 km length in Brazil during the same period of time (Wanninger, 1993). Investigation of anomalous ionospheric gradients discovered by

* Corresponding author at: Civil Engineering Department, Faculty of Engineering, Ferdowsi University of Mashhad (FUM), Mashhad, Razavi Khorasan Province, Iran. Tel.: 9177948974.
E-mail address: etemadfard@um.ac.ir (H. Etemadfard).

https://doi.org/10.1016/j.asr.2020.12.023
0273-1177/

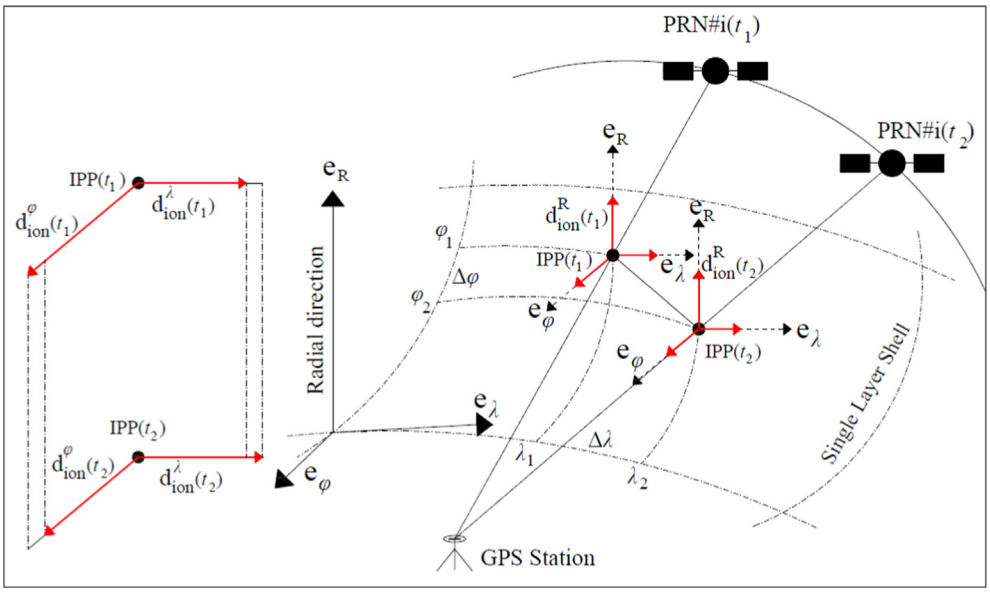

Fig. 1. Schematic view of spatial gradient computation between two successive epochs.

the Wide Area Augmentation System (WAAS) has reported gradients as large as hundreds of mm/km (or hundreds of parts per million), which is far larger than typical ionospheric gradients of 1–5 mm/km (Datta-Barua et al., 2002). Others have shown larger gradients during the sever ionospheric storms of October and November 2003 (Ene et al., 2005; Datta-Barua et al., 2010). Some studies demonstrate that horizontal gradients of ionosphere can affect GPS coordinates significantly in both single point and differential positioning modes (Abdullah et al., 2007). In differential GPS positioning ionospheric delay is dependent on the baseline direction. As the result, spatial changes in the ionosphere can increase or decrease as compared to the case where the existing gradients are ignored (Abdullah et al., 2007). Since, the error due to the ionospheric refraction is assumed to be the same for two closely spaced signal paths, the presence of ionospheric horizontal gradient is normally ignored. If the signal path is exposed to a drastically large ionospheric gradient (e.g., over the equatorial region), the large difference of ionospheric delays between the reference and user stations can result in significant positioning error at the user's position (Nagarajoo and Zain, 2010). In other words, gradient of ionosphere has significant effect on baselines that are 100 km and more. Typically, large-scale gradients in Total Electron Content (TEC) can result in differential ionosphere range delays of about 1–2 ppm (Parkinson and Enge, 1996).

Real Time Kinematic (RTK) networks are now an efficient solution for many of the industrial demands on real time position. As the result, the ionospheric storms and their associated ionospheric gradients have been assessed on the relevant solutions (Stankov and Jakowski, 2006): RTK corrections for positioning services including the Satellite-Based Augmentation System (SBAS) used in Australia, as a solution for Intelligent Transport Systems (ITS) (Imparato et al., (2018)) and the U. S. Nationwide Differential Global Positioning System (NDGPS) can be mentioned to name a few (Hirokawa and Fujita, 2019). Then the corrections are applied based on the error range that is sent to the roving receivers (Kintner and Ledvina, 2005). The ionospheric gradients are analyzed seasonally in order to give input information to the threat modeling process over Turkey (Koroglu et al., 2017). Other researches have tried to estimate the influence of the spatial gradient on ionospheric mapping using globally distributed GNSS stations and the NeQuick2 ionospheric electron density model (Jiang et al., 2018). In a recent research, the ionospheric temporal gradient analysis has been carried out in east, west, north and south directions using a Weighted Least Squares (WLS) algorithm for NAVIC (Navigation with Indian Constellation (NAVIC)) L5 signals (Kumar et al., 2019).

Various models have been suggested for estimating ionospheric parameters using the GNSS measurements in global, regional and local scales (Schunk et al., 2004; Bilitza and Reinisch, 2007; Hochegger et al., 2000; Komjathy, 1997; Schaer, 1999; Schmidt, 2007; Etemadfard and Hossainali, 2016a; Zhang et al., 2019). Other methods have been also suggested for computing the spatial gradient of ionosphere (Lee et al., 2007; Chandra et al., 2009). Application of these methods is limited to small baselines. In other words, it is not possible to use such methods for estimating the spatial gradient of ionosphere over large distances. Recently, a new method has been suggested for simultaneous modeling of the spatial gradients of ionosphere and VTECs using vector ionosphere modeling in the Arctic region (Etemadfard and Hossainali, 2016b). The method is based on the spherical shell approximation of ionosphere and models the TEC

in the radial and the gradient of TEC in tangential directions. Vector Spherical Slepian (VSS) theory has been suggested for the development of these functions (Etemadfard and Hossainali, 2016b). The VSS theory is the extension of Slepian's spatio-spectral concentration problem to vector fields on the sphere. The theory of spatio-spectral concentration is concerned with the optimal space localization of a signal bandlimited in the frequency domain. Simons et al. (2006; 2009) and Simons (2010) extended these results on the sphere for bandlimited functions in the Spherical Harmonics (SHs) domain. Plattner and Simons have presented a complete extension of Slepian's spatio-spectral concentration problem to vector fields on the sphere (Platner and Simons, 2014). Etemadfard and Hossainali (2015) applied this method for improving the accuracy of the IGS Global Ionosphere Models (GIMs) in polar region. Then, Etemadfard and Hossainali proposed the spherical Slepian base functions as a new method for modeling the VTEC in the Arctic region (2016a).

This study intends to simultaneously compute the spatial gradients of ionosphere and VTECs over Iran. Observations of the national GPS network and the VSS method have been used for this purpose. This new experiment is challenging in several aspects; the case study is the first attempt to the application of this method for modeling the ionosphere in mid latitude region. Here, the gradients of ionosphere are expected to have smaller impacts on GPS measurements. The size of the new test area is also smaller than the test area in our previous research (Etemadfard and Hossainali, 2016b). This provides a new opportunity for evaluating the effect of VSS modeling on the GPS baseline solutions. In addition, since the Slepian base functions are linear combination of Vector Spherical Harmonics (VSH), a new optimal set of the required base functions have been developed for the test area of the present research. Results of this study can therefore, provide an initial insight onto the contribution of ionospheric gradients on practical applications such as the development of a real time positioning service in mid latitude region. In contrary to Arctic region, the shape of study area is highly irregular in this new experiment. Due to the irregular boundary of the test area, the modeling of VSS base functions and using them must be changed.

Application of this method requires an appropriate set of input data. To this end, GPS measurements are firstly used to determine Slant TEC (STEC) at every Ionospheric Pierce Point (IPP). Using numerical differentiation, gradient of STEC is computed in the longitudinal and latitudinal directions (Etemadfard and Hossainali, 2016b).

The vector Slepian theory is introduced in the next section of this research (Section 2.1). The method that is applied for the construction of input data is given next (Section 2.2). Section 3 presents the corresponding numerical results. Pros and cons of the proposed method are discussed in this section. Finally, Section 4 gives the concluding remarks.

2. VSS function modeling

This research is a function based method for the vectorial modeling of ionosphere in local scale. The applied base functions are based on the Slepian's spatio-spectral concentration extended to VSH fields on unit sphere (Platner and Simons, 2014). Therefore, the VSS theory and the analytical equations for the derivation of the corresponding base functions are given first. Then, the method is explained for constructing input data.

2.1. VSS base functions

Platner and Simons (2014) firstly suggested the VSS base functions for bandlimited vector fields, $\boldsymbol{g}(\hat{\boldsymbol{r}})$ on the unit sphere Ω:

$$\boldsymbol{g}(\hat{\boldsymbol{r}}) = \boldsymbol{g}^{r}(\hat{\boldsymbol{r}}) + \boldsymbol{g}^{t}(\hat{\boldsymbol{r}}) = \sum_{lm}^{K} U_{lm}\boldsymbol{P}_{lm} + V_{lm}\boldsymbol{B}_{lm} + W_{lm}\boldsymbol{C}_{lm} \quad (1)$$

$$\boldsymbol{P}_{lm} = \hat{\boldsymbol{r}}Y_{lm},\ \boldsymbol{B}_{lm} = \frac{\nabla_1 Y_{lm}}{\sqrt{l(l+1)}}, \boldsymbol{C}_{lm} = \frac{-\hat{\boldsymbol{r}}\times\nabla_1 Y_{lm}}{\sqrt{l(l+1)}} \quad (2)$$

$$U_{lm} = \int_{\Omega} \boldsymbol{P}_{lm}.\boldsymbol{g}d\Omega,\quad V_{lm} = \int_{\Omega} \boldsymbol{B}_{lm}.\boldsymbol{g}d\Omega,\quad and$$
$$W_{lm} = \int_{\Omega} \boldsymbol{C}_{lm}.\boldsymbol{g}d\Omega. \quad (3)$$

where Y_{lm} is the SH base function for degree l, order m and maximum degree K. Here, ∇_1 is the tangential part of the gradient. Unit vectors $\widehat{\theta}$ and $\widehat{\lambda}$ are in the south and east directions, respectively. The VSS theory is taken from the scalar Slepian theory and it maximize the spatial concentration it within R via the ratio:

$$\lambda = \frac{\boldsymbol{g}^{T}\boldsymbol{K}\boldsymbol{g}}{\boldsymbol{g}^{T}\boldsymbol{g}}, \boldsymbol{g} = [\ldots, U_{lm}, \ldots, V_{lm}, \ldots, W_{lm}, \ldots]^{\mathrm{T}} \quad (4)$$

where **K** is real, symmetric, and positive definite matrix with $[3(K+1)^2-1]\times[3(K+1)^2-1]$-dimension. It can be divide to sub matrices like,

$$\boldsymbol{K} = \begin{bmatrix} \boldsymbol{P} & \boldsymbol{0} & \boldsymbol{0} \\ \boldsymbol{0} & \boldsymbol{B} & \boldsymbol{D} \\ \boldsymbol{0} & \boldsymbol{D}^{T} & \boldsymbol{C} \end{bmatrix} \quad (5)$$

In this equation, **P** is the radial part of the vector field, which is equal to

$$\boldsymbol{P} = \begin{bmatrix} P_{00,00} & \cdots & P_{00,KK} \\ \vdots & \ddots & \vdots \\ P_{KK,00} & \cdots & P_{KK,KK} \end{bmatrix}, \quad P_{lm,l'm'} = \int_{R} Y_{lm}.Y_{l'm'}d\Omega. \quad (6)$$

In the similar way, the entry of **B**, **C** and **D** will be such as

$$\boldsymbol{B}=\begin{bmatrix} B_{10,10} & \cdots & B_{10,KK} \\ \vdots & \ddots & \vdots \\ B_{KK,10} & \cdots & B_{KK,KK} \end{bmatrix}, \boldsymbol{C}=\begin{bmatrix} C_{10,10} & \cdots & C_{10,KK} \\ \vdots & \ddots & \vdots \\ C_{KK,10} & \cdots & C_{KK,KK} \end{bmatrix},$$
$$\boldsymbol{D}=\begin{bmatrix} D_{10,10} & \cdots & D_{10,KK} \\ \vdots & \ddots & \vdots \\ D_{KK,10} & \cdots & D_{KK,KK} \end{bmatrix},$$
$$B_{lm,l'm'}=\int_R \boldsymbol{B}_{lm}.\boldsymbol{B}_{l'm'}d\Omega,\quad C_{lm,l'm'}=\int_R \boldsymbol{C}_{lm}.\boldsymbol{C}_{l'm'}d\Omega,$$
$$D_{lm,l'm'}=\int_R \boldsymbol{B}_{lm}.\boldsymbol{C}_{l'm'}d\Omega. \tag{7}$$

Based on Equation (4), it is possible to construct an orthogonal family of bandlimited eigenfields that is optimally concentrated within a region R on the unit sphere Ω, by solving the matrix eigenvalue problem below

$$\boldsymbol{K}\boldsymbol{g}=\lambda\boldsymbol{g} \tag{8}$$

Its eigenvalues can be sorted from one to zero and eigenvectors are orthogonal. This method determine the optimally concentrated eigenfields in the region R. Each VSS function is distinguished by two indices. The first is *m*which is equivalent to the order of the corresponding VSH and the second is α which is called the degree of a VSS function here, although it cannot be directly compared to the degree of VSHs or the concept of degree in a polynomial as well. For more details, the reader is referred to read Platner and Simons (2014)and use https://github.com/Slepian/Slepian to implementation.

2.2. Input data

The required input data are prepared with the dual-frequency GPS observations. Carrier phase smoothed codes $\widetilde{P}_1$ and $\widetilde{P}_2$ are applied for this purpose. This is done using (Dach et al., 2007),

$$\widetilde{P}_1(t)=\phi_1(t)+\bar{P}_1-\bar{\phi}_1+\frac{2f_2^2}{f_1^2-f_2^2}\left(\left(\phi_1(t)-\bar{\phi}_1\right)-\left(\phi_2(t)-\bar{\phi}_2\right)\right)$$
$$\widetilde{P}_2(t)=\phi_2(t)+\bar{P}_2-\bar{\phi}_2+\frac{2f_1^2}{f_1^2-f_2^2}\left(\left(\phi_1(t)-\bar{\phi}_1\right)-\left(\phi_2(t)-\bar{\phi}_2\right)\right). \tag{9}$$

In this equation$\phi_f(t)$ is the carrier phase measured at epoch t using frequency$f$, $\bar{P}_f-\bar{\phi}_f$ is the mean difference between all the accepted code and phase measurements in the current observation arc on frequency f, and f_1 and f_2 are the carrier frequencies for observation ϕ_1 and ϕ_2, respectively. To compute the ionospheric delays at epoch t, the bellow relation is used;

$$d_{ION}(t)=\widehat{P}_2(t)-\widehat{P}_1(t) \tag{10}$$

Then, $d_{ION}(t)$ is projected onto the east–west, north–south and radial directions by using the equations (Etemadfard and Hossainali, 2016b),

$$\begin{aligned} d^{\lambda}_{ION}(t)&=d_{ION}(t)\cos(EL')sin(AZ)\\ d^{\varphi}_{ION}(t)&=d_{ION}(t)\cos(EL')\cos(AZ)\\ \cos(EL')&=\tfrac{R}{R+H}\cos(EL)\\ d^{R}_{ION}(t)&=d_{ION}(t)\sin(EL') \end{aligned}, \tag{11}$$

whereEL and AZ are the elevation angle and azimuth of the satellite at the receiver position, and $d^{\lambda}_{ION}(t)$, $d^{\varphi}_{ION}(t)$and $d^{R}_{ION}(t)$ are the east–west, north–south and radial components of ionospheric delay, respectively. R and H are the earth's mean radius (6371 km) and the single layer altitude, which is 450 km in this research. The radial component of ionospheric delay can be used to compute the TEC in radial direction. This is done as,

$$TEC^{R}(t)=\frac{f_1^2f_2^2d^{R}_{ION}(t)}{40.3\left(f_1^2-f_1^2\right)} \tag{12}$$

for epoch t. In order to compute tangential gradients of ionospheric delay, tangential gradients of TEC (ΔTEC^{λ}&ΔTEC^{φ}) are required as input data. ΔTEC^{λ} and ΔTEC^{φ} are computed utilizing Newton's difference quotient or the first order divided difference formulae (Etemadfard and Hossainali, 2016b),

$$\begin{aligned} \Delta TEC^{\lambda}()&=\tfrac{f_1^2f_2^2}{40.3\left(f_2^2-f_1^2\right)\Delta\lambda}\left(d^{\lambda}_{ION}(t_2)-d^{\lambda}_{ION}(t_1)\right)\\ \Delta TEC^{\varphi}(t_1)&=\tfrac{f_1^2f_2^2}{40.3\left(f_2^2-f_1^2\right)\Delta\varphi}\left(d^{\varphi}_{ION}(t_2)-d^{\varphi}_{ION}(t_1)\right) \end{aligned} \tag{13}$$

Where t_1 and t_2 are two successive epochs. This method can be shown by the below figure.

Although $d^{\lambda}_{ION}(t)$and $d^{\varphi}_{ION}(t)$ depend on the azimuth and elevation of the GNSS satellites, application of equation (13) helps ignore this dependency in the method of this research. This is because these parameters are almost the same at the corresponding pierce points. In other words, the EL and AZ difference between the two sequential epochs is so small and is skipped in the calculations of equation (13).

3. Numerical result

This section firstly introduces the study area, the process of selection and preparation of input data. The next subsection discusses the generation of the new base functions in complete detail. Finally, developed models are given and compared together.

3.1. GPS array and the input data

For the assessment of introduced method, 28 permanent GPS stations from the Iranian Permanent GPS Network (IPGN) have been selected and used in this research. The sampling rate of measurements is 30 s and the elevation cut-off angle is 30°. Totally 24 stations (control stations) are used for developing the gradient models. In other words, using the observations of these stations the model coefficients are estimated for the study area of this research.

Remaining stations (check stations) are used for the evaluation of proposed method. Fig. 2 illustrates the distribution of the control and check stations.

For reasonable analysis of the accuracy of developed models, a period should be selected for the experiment. This period should include both the high and low geomagnetic activities. The Kp-index as an indication for geomagnetic activity caused by the sun is used for this purpose. According to the finalized Kp-index reported by the GFZ Potsdam, 10 days starting from 06.03.2012 (DOY 66) and ending on 15.03.2012 (DOY 75) has been selected as the time period. There are the days of high and low geomagnetic activity in this time duration.

Satellites' Differential Code Biases (DCBs) are available through the Center of Orbit Determination in Europe (CODE). The receivers' DCBs are computed in the preprocessing step. Input data are computed by Equation (12) and (13)). Moreover, coordinates of the IPPs , the intersection of the GPS signals with a single layer shell located at an altitude of $H = 450$ Km above the surface of the Earth are necessary for developing the regional models since the IPP coordinates (φ, λ) are the inputs of ionospheric models. Fig. 3a and 3b illustrate the IPPs' position for the control and check stations, respectively.

The Least Squares (LS) method is used for the estimation of unknown parameters. Based on the error propagation rule, the weight matrix is also estimated for the application in the LS procedure. These equations are also applied to the observations of the check points for analyzing the accuracy of developed models.

3.2. Model analysis

In this research, the coefficients of models are estimated in every measurement epoch. To be more specific, input data, i.e. VTECs and its spatial gradients, are computed from every successive epochs (e.g. epochs n, n + 1). This input is then used for the estimation of the VSS coefficients at the desired epoch (e.g. epoch n). Similarly, VTECs and the gradients that are computed at the check stations are employed to analyze the accuracy of developed models. Root Mean Square Errors (RMSEs) are computed for each model during the entire period in question. For further analysis, daily averages of RMSEs are also calculated for the developed models. Analysis of this parameter provides a deeper insight into the efficiency of each model as compared to the others. Fig. 4 illustrates the daily averages of RMSEs in TECU/degree at the East-West direction. TECU is the TEC Unit that equals to 10^{16} electron/m^2.

According to Fig. 4, the RMSE of the model is consistently larger when $K = 30$ and $K = 50$. Moreover, the model performs more accurately when $K = 40$. Based on the obtained results, the overall average of RMSEs are 0.092, 0.085, 0.066, 0.088, 0.112 TECU/degree for K equal to 30, 35, 40, 45 and 50, respectively. Next, the daily aver-

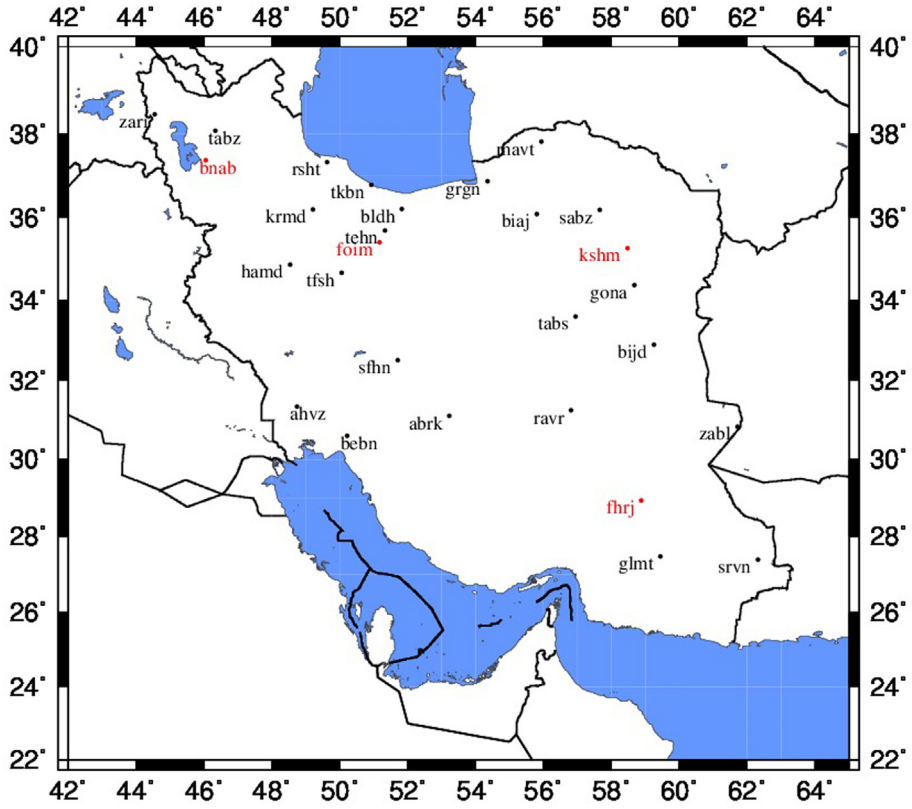

Fig. 2. Control and check stations in black and red, respectively. (For interpretation of the references to colour in this figure legend, the reader is referred to the web version of this article.)

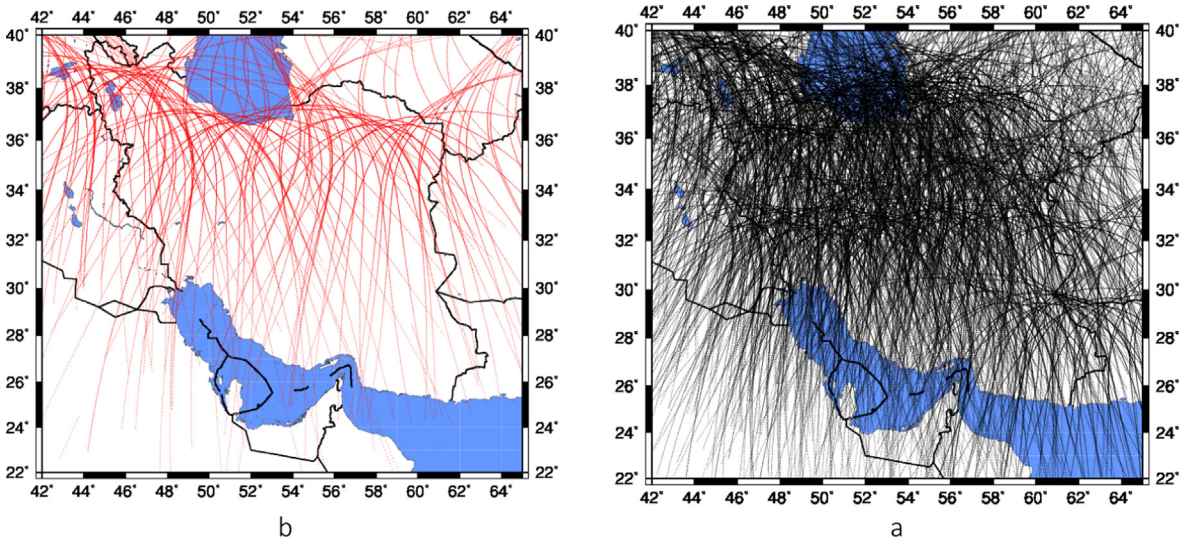

Fig. 3. The IPPs of the control (a) and check stations (b).

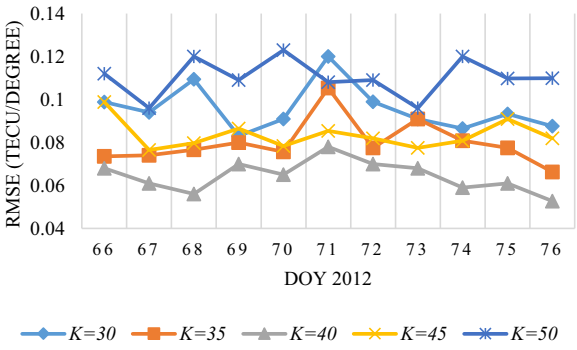

Fig. 4. The daily averages of RMSEs in the East-West component by using different K.

ages of RMSEs are computed in the North-South direction. Fig. 5 illustrates the obtained results.

Similar conclusions can be drawn from Fig. 5. According to this figure, $K = 40$ is the best selection for the maximum degree of the model in the North-South direction as compared to the other proposed values. The corresponding results in the East-West direction are similar to the North-South direction for the other models. Finally, daily averages of RMSEs are also computed in the radial direction (VTEC). Fig. 6 illustrates the obtained results.

It is found out that $K = 35$ and 40 have the same results. It means that both of them can be used for ionospheric modeling in the radial direction. According to the result obtained at the tangential directions, $K = 40$ has been preferred to $K = 35$ in this study. This is the optimum maximum degree for the ionospheric VSS modeling over Iran.

It can be found that different geomagnetic activities and ionospheric perturbation do not have an important role in this kind of modeling (epoch-wise). In addition to that, the under-fitting and over-fitting occurs when K is equal to 30 and 50, respectively.

In order to analyze the efficiency of developed model, it has been applied to a DGPS positioning mission. The baseline repeatability is chosen as the required measure for this purpose. To this end, four baselines have been taken into account: The shortest baseline is tehn-foim, two long baselines in the east–west (ahvz-zabl) and north–south (mavt-glmt) orientation and srvn-zari which is the longest baseline in this research. The spatial distribution and the baseline lengths are given in Fig. 7.

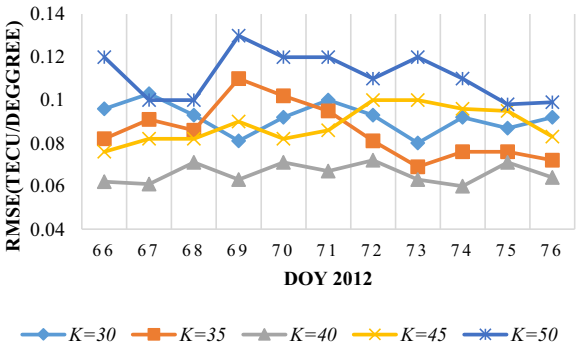

Fig. 5. The daily averages of RMSEs in the North-South component by using different K.

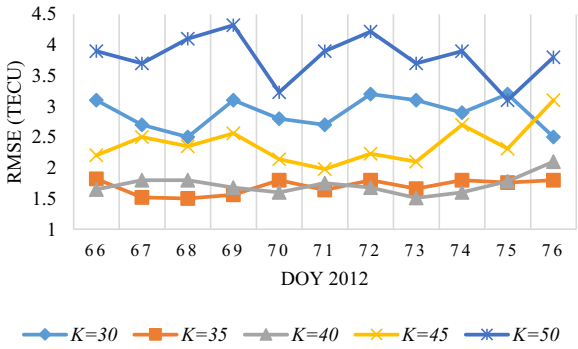

Fig. 6. The daily averages of RMSEs in the Radial component by using different K.

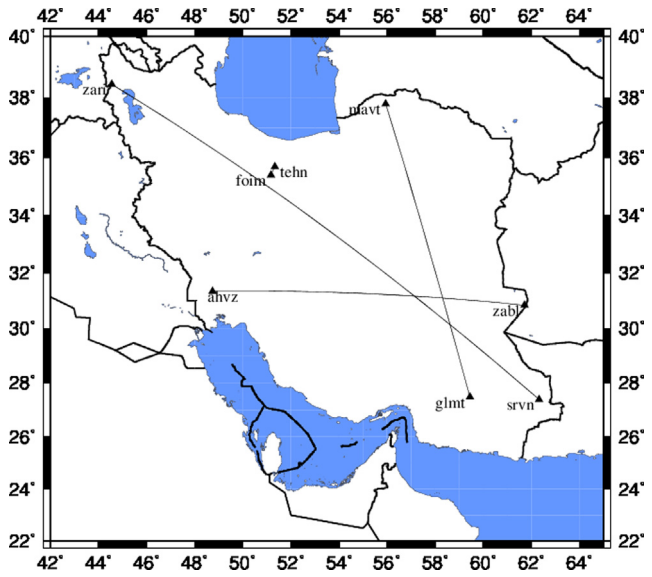

Fig. 7. Spatial distribution of the shortest baseline tehn-foim (35 Km), the east–west baseline ahvz-zabl (1236Km), the north–south baseline mavt-glmt (1188Km) and the longest baseline srvn-zari (2216Km) in the experiment of this research.

Repeatability of these baselines is analyzed using epoch wise single frequency pseudo-range baseline (single difference) solutions. RTKlib is used for this purpose (Takasu, 2011). Raw observations are firstly used to compute the baseline solutions without ionospheric correction (see the row 'off' in Tables 1–3). For the assessment of the role of Equation (13) which shows the direct gradient of observation, the horizontal derivatives of the radial direction have been taken into account for TEC gradient. Next, input data are corrected for ionospheric error using the VSS model of this research (see the row 'VSS' in Tables 1–3). Finally, ionospheric free linear combination has been used as a benchmark for this analysis (see the row 'free-ion' in Tables 1–3). Table 1 illustrates the results obtained for the east–west component.

According to Table 1, the shortest baseline is not affected by ionospheric delay. The east–west component of ahvz-zabl and mavt-glmt baselines has improved about 9% and 7%, respectively. The improvement is 12% in the longest baseline in the east–west component. Table 2 shows the results for north–south component.

Based on Table 2, the tehn-foim, ahvz-zabl and mavt-glmt baselines have 3%, 10% and 16% improvements, respectively when the VSS has been used. In addition to that, the rule of directly using the raw differential observation is vividly impressive. Moreover, the longest baseline has significant improvement of about 18%. Table 3 reports on the up-down component for this baseline.

Table 1
Repeatability of the baseline in the east–west component in meter.

Baseline	tehn-foim	ahvz-zabl	mavt-glmt	srvn-zari
off	1.62	3.28	2.03	5.56
horizontal derivatives	1.6	3.11	1.94	5.23
VSS	1.6	2.98	1.88	4.89
free-ion	1.6	2.47	1.78	3.37

Table 2
Repeatability of the baseline in the north–south component in meter.

Baseline	tehn-foim	ahvz-zabl	mavt-glmt	srvn-zari
off	1.86	3.87	2.6	4.41
horizontal derivatives	1.82	3.74	2.41	3.98
VSS	1.8	3.48	2.18	3.58
free-ion	1.75	2.75	1.71	3.31

Table 3
Repeatability of the baseline in the up-down component in meter.

Baseline	tehn-foim	ahvz-zabl	mavt-glmt	srvn-zari
off	1.68	4.44	2.24	5.48
horizontal derivatives	1.68	4.35	2.18	5.19
VSS	1.68	4.08	2.09	4.94
free-ion	1.67	3.53	1.96	4.18

Table 3 shows that, VSS model doesn't have any impact on short baselines. The repeatability parameter on ahvz-zbl and mavt-glmt displays an improvement of about 7% for using VSS method. It is equal to 10% for srvn-zari baseline as the biggest baseline. Moreover, these results show that Eq. (13) has significant impact for vector ionospheric modeling.

4. Conclusion

This research applies a new method for vector ionosphere modeling over on the irregular area. The method has been applied to the GPS data in Iran as the test area. Proposed method is based on the VSS base functions. The method provides an epoch wise solution to the problem of modeling the ionosphere. Because of this property, geomagnetic activities and ionospheric perturbation don't have any important impact on the corresponding products.

To come up with an optimum model, five different maximal degrees ($K = 30, 35, 40, 45$ & 50) are taken into account. Based on the results, $K = 40$ have been chosen as the optimum maximum degree for the ionosphere model in Iran.

The efficiency of the VSS approach have been evaluated by using four baselines. This shows that the ionospheric gradients have more influence on the north–south component. Moreover, the spatial gradient is negligible in the east–west and up-down components on short baselines. The proposed approach to modeling ionosphere has significant application on long baselines. According to the result obtained, the VSS method improves the repeatability of the long baselines' solution more than 12%, 18% and 10% in east–west, north–south and up-down components, respectively.

Declaration of Competing Interest

The authors declare that they have no known competing financial interests or personal relationships that could have appeared to influence the work reported in this paper.

References

Abdullah, M., Strangeway, H.J., Walsh, D.M.A., 2007. Effects of ionospheric horizontal gradients on differential GPS. Acta Geophys. 55 (4), 509–523. https://doi.org/10.2478/s11600-007-0029-z.

Bilitza, D., Reinisch, B., 2007. International Reference Ionosphere 2007: Improvements and new parameters. Adv. Space Res. 42, 599–609.

Chandra, K.R., Srinivas, V.S., Sarma, A.D., 2009. Investigation of ionospheric gradients for GAGAN application. Earth Planets Space 61 (5), 633–635.

Dach, R., Hugentobler, U., Fridez, P., Meindl, M., 2007. Bernese GPS Software version 5.0. Astronomical Institute. University of Berne, Switzerland.

Danilogorskaya, E.A., Zernov, N.N., Gherm, V.E., Strangeways, H.J., 2017. On the determination of the effect of horizontal ionospheric gradients on ranging errors in GNSS positioning. J. Geod. 91 (5), 503–517.

Datta-Barua, S., Lee, J., Pullen, S., LuoM, EneA, Qiu, D., ZhangG, Enge P, 2010. Ionospherethreat parameterization for local area global positioning system-based aircraft landing system. Journal of Aircraft 47 (4), 1141–1151.

Datta-Barua S, Walter T, Pullen S, Luo M, Blanch J, Enge P (2002) Using WAAS Ionospheric Data to Estimate LAAS Short Baseline Gradients. Proceedings of the Institute of Navigation NationalTechnical Meeting, Inst. of Navigation, Alexandria, VA, 2002,pp. 523–530.

Ene, A., Qiu, D., Luo, M., Pullen, S., Enge, P., 2005. In: A comprehen-siveionosphere storm data analysis method to support LAAS threat-model development. Institute of Navigation, San Diego CA, pp. 110–130.

Erickson, W.C., Perley, R.A., Flatters, C., Kassim, N.E., 2001. Iono-spheric corrections for VLA observations usingLocal GPS data. Astronomy & Astrophysics A&A 366, 1071–1080. https://doi.org/10.1051/0004-6361:20000359.

Etemadfard, H., Hossainali, M.M., 2015. Application of Slepian theory for improving the accuracy of SH-based global ionosphere models in the Arctic region. J. Geophys. Res. Space Phys. 120. https://doi.org/10.1002/2015JA021811.

Etemadfard, H., Hossainali, M.M., 2016a. Spherical Slepian as a new method for ionospheric modeling in Arctic region. J. Atmos. Sol. Terr. Phys. 140, 10–15. https://doi.org/10.1016/j.jastp.2016.01.003.

Etemadfard, H., Hossainali, M.M., 2016b. Vector Ionosphere Modeling by Vector Spherical Slepian Base Functions. GPS Solution.

Goad, C.C., 1990. Optimal Filtering of Pseudoranges and Phases from Single-Frequency GPS Receivers. Navigation 37 (3), 249–262.

Hirokawa, R., & Fujita, S. (2019). A Message Authentication Proposal for SatelliteBased Nationwide PPP-RTK Correction Service. In Proceedings of the 32nd International Technical Meeting of the Satellite Division of The Institute of Navigation (ION GNSS+ 2019) (pp. 1798-1811).

Hochegger, G., Nava, B., Radicella, S., Leitinger, R., 2000. A family of ionosphericmodels for different uses. Phys. Chem. Earth Part C Sol. Terr. Planet Sci. 25, 307–310.

Imparato, D., El-Mowafy, A., Rizos, C., Wang, J., 2018. Vulnerabilities in SBAS and RTK positioning in intelligent transport system: An overview. In Proceedings of the International Global Navigation Satellite System Association IGNSS Symposium.

Jiang, H., Wang, Z., An, J., Liu, J., Wang, N., Li, H., 2018. Influence of spatial gradients on ionospheric mapping using thin layer models. GPS Solutions 22 (1), 2.

Kintner, P.M., Ledvina, B.M., 2005. The ionosphere, radio navigation, and global navigation satellite systems. Adv. Space Res. 35 (5), 788–811.

Komjathy, A., 1997. Global ionospheric total electron content mapping using the global positioning system. Ph.D dissertation, Department of Geodesy and Geomatics Engineering, Technical Report No. 188. University of New Brunswick, Canada, p. 248.

Koroglu, M., Koroglu, O., Arikan, F., 2017. Analysis of seasonal ionospheric gradients over Turkey for year 2011. In: 2017 XXXIInd General Assembly and Scientific Symposium of the International Union of Radio Science (URSI GASS). IEEE, pp. 1–4.

Kumar, M.R., Sridhar, M., Ratnam, D.V., Harsha, P.B.S., Sri, S.N., 2019. Estimation of ionospheric gradients and vertical total electron content using dual-frequency NAVIC measurements. Astrophys. Space Sci. 364 (3), 49.

Lee J, Pullen S, Datta-Barua S, Enge P, 2007. Assessment of Ionosphere Spatial Decorrelation for GlobalPositioning System-Based Aircraft Landing Systems. JOURNAL OF AIRCRAFTVol. 44, No. 5, September–October.

Liu J, Kuga Y, Ishimaru A, Pi X, Freeman A., 2003. Ionospheric Effects on SAR Imaging:A Numerical Study. IEEE TRANSACTIONS ON GEOSCIENCE AND REMOTE SENSING, VOL. 41, NO.5, MAY 2003 939.

Meyer F, Bamler R, Jakowski N, Fritz T., 2005. The Potential of Broadband L-Band SAR Systems for Small Scale Ionospheric TEC Mapping", in Lacoste, H., ed., Proceedings of Fringe 2005 Workshop, Frascati, Italy, ESA Special Publications, SP- 610, (ESA Publications Division, Nordwijk, 2006).

Nagarajoo, K., Zain, A.F.M., 2010. In: DGPS positional improvement by mitigating the ionospheric horizontal gradient and elevation angle effects. IEEE, pp. 1–4.

Parkinson, B.W., Enge, P.K., 1996. Differential GPS. Global Positioning Syst. Theory Appl. 2, 3–50.

Platner, A., Simons, F.J., 2014. Spatiospectral concentration of vector fields on a sphere. Appl. Comput. Harmon. Anal. 36 (1), 1–22.

Schaer, S., 1999. Mapping and predicting the Earth's ionosphere using the Global Positioning System. Bern University, Switzerland, Ph.D. thesis.

Schmidt, M., 2007. Wavelet modeling in support of IRI. Adv. Space Res. Off. J. Committeeon Space Res. (COSPAR) 39, 932–940.

Schunk R, Scherliess L, Sojka J. Thompson D (2004) Global assimilation of ionospheric measurements (GAIM). Radio Sci., 39.

Simons F J (2010) Slepian functions and their use in signal estimation and spectral analysis.in Handbook of Geomathematics (W. Freeden, M. Z. Nashed, andT. Sonar, eds.) Heidelberg, Germany: Springer, ch. 30, pp. 891–923,doi: 10.1007/978–3–642–01546–5 30.

Simons, F.J., Dahlen, F.A., Wieczorek, M.A., 2006. Spatiospectral concentration on a sphere. SIAM Rev. 48 (3), 504–536. https://doi.org/10.1137/S0036144504445765.

Simons F J, Hawthorne J C, Beggan C D (2009) Efficient analysis and representation of geophysical processes using localized spherical basis functions. in Wavelets XIII (V. K. Goyal, M. Papadakis, and D. Van de Ville, eds.), vol. 7446, pp. 74460G, doi: 10.1117/12.825730, SPIE.

Stankov, S.M., Jakowski, N., 2006. Ionospheric effects on GNSS reference network integrity. J. Atmos. Solar Terr. Phys. 69 (4–5), 485–499.

Takasu T (2011) RTKLIB: an open source program package for GNSS positioning (11 June 2011). http://www.rtklib.com/prog/rtklib_2.4.2.zip

Wanninger L (1993) Effects of the Equatorial Ionosphere on GPS. GPS World, July.

Zhang, Z., Pan, S., Gao, C., Zhao, T., Gao, W., 2019. Support Vector Machine for Regional Ionospheric Delay Modeling. Sensors 19 (13), 2947.